Extraction of Vessels Networks over an Orientation Domain

Mickaël Péchaud, Gabriel Peyré, Renaud Keriven

Extraction of Vessels Networks
over an Orientation Domain

Mickaël Péchaud
DI
École Normale Supérieure
France

Gabriel Peyré
CEREMADE, CNRS
Université Paris-Dauphine
France

Renaud Keriven
CERTIS - École des Ponts
Université Paris-Est
France

November 10, 2008

Abstract

This paper presents a new method to extract a network of vessels centerlines from a medical image. The network is composed of local geodesics over a four-dimensional space that includes local orientation and scale. These shortest paths follow closely the center of tubular structures and can deal robustly with crossings over the image plane. The vessel network is grown by an iterative algorithm that distributes seed points according to a geodesic saliency field. Numerical experiments on a database of synthetic and medical images show the superiority of our approach with respect to several methods based on shortest paths extractions. With a minimum of user interaction, it allows to compute a complex network of vessels over noisy medical.

1 Introduction

Detection of vessel networks in images is of primary interest to help medical diagnostic. The extraction of an accurate network allows one to compute meaningful information such as the local width of the vessels and the connectivity of the networks from a single planar observation.

Crossings and occlusions in 2D medical images are challenging problems that cannot be overcome by a local search procedure. This paper recasts the 2D extraction problem as a geodesic computation over a 4-dimensional space. An additional scale dimension gives access to the local width of the vessels, and allows the direct extraction of the centerline of the vessel. A rotational dimension reduces erroneous detection when two vessels are overlapping. Numerical experiments show the superiority of our approach with respect to state-of-the-art geodesic based methods. A network extraction method relying on this framework is then proposed, and experimented on several real and synthetic medical images.

1.1 Previous Work

The problem of vessels extraction has received considerable attention in the computer vision and medical imaging communities - see for instance the recent review by Kirbas and Quek [24], or [16] for further references. Several class of methods have been proposed to segment vessels in medical images. They generally rely on the use of a local detector, postprocessed by a method that links locally detected vessels.

Local detectors allow to detect points belonging to vessels or portions of vessels depending on the modality of the image. Local detectors include various methods: thresholding of images intensities, ridge or crest detection [1, 36, 5], wavelets [21, 46, 10], differential operators [33, 27], gabor filters [38] or matching filters [15, 7, 20, 3, 6, ?, ?].

Many methods allow to link or post-process the locally detected points.

Among classical methods (inspired by ideas which early arose in computer vision community for edge detection [4]), thresholding [50], fusion processes [23, 17, 31, 53], region growing algorithms

[13, 42, 55, 19], front propagation [30, 44], or pixel classification [10, 39, 45] techniques were proposed.

Geodesic based methods is another class of methods allowing the linking of local features – usually pixels intensities: the notion of **shortest path** or **geodesic** proved to be efficient for the extraction of salient curves in 2D or 3D images, see for instance [9, 34]. Geodesic curves can also be used to extract tubular structure centerlines in 3D, as proposed by Deschamps and Cohen [12] and by Santamaria et al [40]. Li and Yezzi [28] proposed to extend the shortest path computation to a higher dimensional domain. They include local radius of the vessels as an additional scale dimension in order to stabilize the computations and to select the centerline without any post-processing.

Another way of linking local features is the class of **tracking methods** which start from a point belonging to a vessel (either user-defined, or detected using a ad-hoc method with respect to the modality), and iteratively track the vessel by analyzing the neighborhood of the current point in the direction of the vessel (look-ahead) [37, 26, 41, 14, 29, 56, 51, 11, 49]. While some of these methods can handle junctions, they usually fail to deal with crossings – which are an extra difficulty of 2D images.

Our method operates a mix of these categories. It lifts the 2D image in a 4D orientation space using local detectors of vessels at different orientations and scales - the 4D orientation space disambiguates crossing configurations [22]. The method is independent from the local detector used, which can be tuned precisely to the targeted application. Our method then uses a geodesic based formalism to compute optimal paths in this 4D space, leading to a robust global segmentation of vessels. Unlike methods which rely on a post-processing skeletization to compute the centerlines of the vessels [52, 47, 18], our method directly and naturally computes both centerlines and radii of vessels. Finally, we propose to use this segmentation to design an algorithm for network extraction. Based on a tracking on extended neighborhoods, our algorithm handles difficult crossing configurations. [2] recently proposed a similar growing-of-minimal-paths framework, but it is specialized to the segmention of closed curves in 2D and meshing of surfaces in 3D.

1.2 Overview

Our vessel network is computed over a 4D domain that includes both local orientation and scale information. The metric over this lifted space is described in Section 2.

Vessels are computed as shortest paths over the 4D domain. The computation of these geodesics is exposed in Section 3. The performance of this method is evaluated in Section 4 on both synthetic and medical images.

We then define a network as a union of vessels. It is computed by an iterative procedure described in Section 5. Numerical examples on synthetic and medical images (both cortical optical imaging [25] and retinal imaging [32]) show the ability of our method to extract network.

2 Local Scale and Orientation Detection

2.1 Local Vessel Model

A medical image is treated as a 2D function $I : [0, 1]^2 \to \mathbb{R}$. The local geometry of a vessel is captured with a vessel model $M(x) \in \mathbf{R}$ for $x = (x_1, x_2) \in \Lambda = [-\Lambda_1, \Lambda_1] \times [-\Lambda_2, \Lambda_2]$. This model is a 2D pattern that incorporates our prior knowledge about both the cross section of the vessels and the regularity of vessel.

The prior on the cross section of the vessel is included by considering models $M(x_1, x_2) = m(x_2)$ that only depends on a 1D profile m. The prior on the regularity of the vessels corresponds to the ratio Λ_1/Λ_2 of the horizontal and vertical dimensions of the model.

Model cross-section for vessels. A 1D profile adapted to both cortical optical imaging and retinal imaging is defined as

$$m(x_2) = \begin{cases} 1 & \text{for } |x_2| > \Lambda_2/2, \\ \exp(-\alpha\sqrt{(1/2)^2 - (x_2/\Lambda_2)^2}) & \text{otherwise.} \end{cases} \tag{1}$$
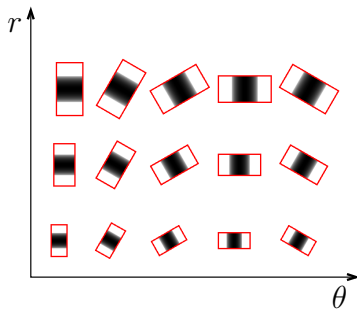
Figure 2: Vessel models for different orientations and scales. Here, $\Lambda_1/\Lambda_2 = 1/2$ and $m(.)$ is given by (1).

This model encompasses medical knowledge about the light reflexion around blood vessels in cortical imaging. The image intensity inside a vessel is assumed to result from a light absorption (with coefficient α) proportional to the vessel width at this point. It is also widely used in the retina image community [7].

The value $\alpha \approx 0.05$ was evaluated from a set of typical cortical images. Section 4.1 shows that our vessel extraction method is robust with respect to approximate choices of this absorption parameter.

Regularity selection. The ratio Λ_1/Λ_2 of the model dimensions acts as a prior on the regularity of typical vessels. The more typical vessels are curved, the smaller Λ_1/Λ_2 should be. Also, robustness to noisy images forces to use a model with a large enough area $\Lambda_1 \times \Lambda_2$. The value of $(\Lambda_1, \Lambda_2) = (1, 2)$ is used in our numerical experiments. It was selected to give the best vessel detection results on a set of exemplar images.

To overcome the inherent difficulties of the 2D detection problem, additional scale and orientation dimensions are introduced to increase the detectability of vessels.

2.2 Rotated and Scaled Models

The normalized pattern $M(x)$ is rotated and scaled to match the varying orientation and width of vessels. Beside the choice of the pattern cross section m and the dimension $\Lambda_1 \times \Lambda_2$ of the model $M(x)$, the scaling of $\Lambda(r)$ with r is another avenue to introduce some prior about vessels in the image. Small scales cortical and retinal vessels are less regular than large scale vessels. We thus chose to scale the dimensions of the model $\Lambda(r) = r\Lambda$ linearly with the radius r. This causes thin tubular structures to be detected using a finer correlation analysis.

The warped model $M_{r,\theta}(x)$ for $x \in \Lambda(r,\theta) = R_\theta \Lambda(r)$ is defined as

$$\forall x \in \Lambda(r,\theta), \quad M_{r,\theta}(x) \stackrel{\text{def.}}{=} M(R_{-\theta}(x/r)) \tag{2}$$

where R_θ is the planar rotation of angle θ.

Figure 2 shows examples of models defined with (1) that are rotated and scaled according to (2).

2.3 Scale/Orientation Lifting

The image I is lifted in a 4D space by adding a scale and an orientation dimension. Let Ω be defined by

$$\Omega \stackrel{\text{def.}}{=} [0,1]^2 \times [R_{\min}, R_{\max}] \times [0, \pi) \tag{3}$$

We call *lifting* the function F computed as the normalized cross-correlation between the image and the local model (2)

$$\forall \omega = (x, r, \theta) \in \Omega, \ F(\omega) \stackrel{\text{def.}}{=} \mathrm{NCC}_{\Lambda(r,\theta)}(M_{r,\theta}(\cdot), I(x + \cdot)) \tag{4}$$

3

where $I(x + \cdot)$ is the image translated by x, $\text{NCC}_A(f, g)$ is the normalized cross-correlation between f and g over the domain A, defined by:

$$\text{NCC}_A(f, g) \stackrel{\text{def.}}{=} \frac{\int_A (f - \bar{f})(g - \bar{g})}{\sqrt{\int_A (f - \bar{f})^2} \sqrt{\int_A (g - \bar{g})^2}} \tag{5}$$

where $\bar{h} = (\int_A h)/|A|$, $|A|$ being the area of A.

This lifting separates real 3D vessels that overlaps when projected at the same location by the imaging system but have different orientations.

The value $F(x, r, \theta)$ ranges from -1 to 1 and measures the likelihood of observing a vessel at a given location x with a width r and an orientation θ. The normalization of the detector makes it invariant under to intensity variations that occurs in medical images due to the elevation variation of the vessels and the imperfection of the imaging system. Adding a scale dimension yiels a robust and regularized estimation if the radius and the center of vessels.

Figure 3 shows an example of a cortical image where orientation lifting is crucial to distinguish locally between orientations.
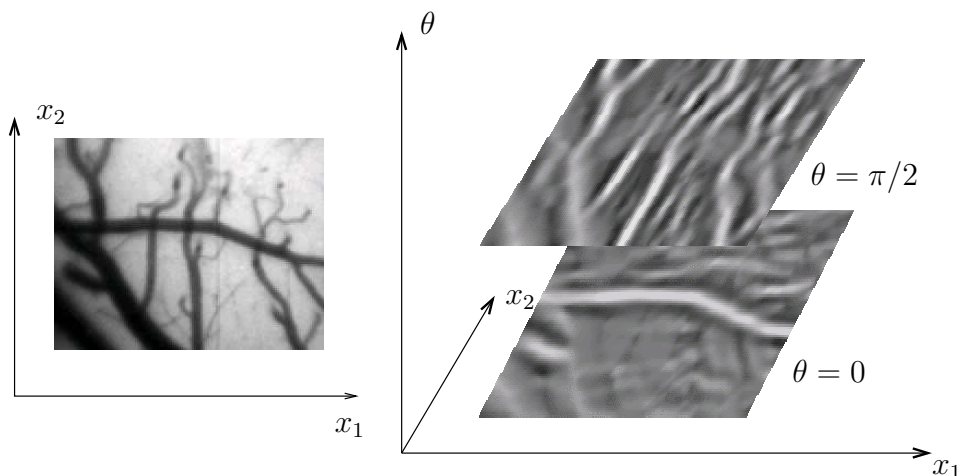

Figure 3: *left:* An original 2D image. *right:* Its 4D lifting (fixed radius), ranging from -1 (black) to 1 (white). White values indicate likely positions and orientations of vessels.

Numerical computations. A medical image is acquired on a on discrete grid of $n \times n$ pixels. The 4D lifting is computed for n_r radii evenly spaced in $[r_{\min}, r_{\max}]$ and n_θ orientations evenly spaced in $[0, \pi)$, with $n_r = 12$ and $n_\theta = 12$ in the experiments. This requires $O((r_{\max} n)^2 n^2 n_r n_\theta)$ operations with $r_{\max} \ll 1$ and $n_r, n_\theta \ll n$.

3 Geodesic 4D curves

3.1 Lifted Metric

The 4D lifting (4) defines an isotropic metric ρ over the 4D domain Ω

$$\forall \omega \in \Omega, \quad \rho(\omega) = \max(1 - F(\omega), \varepsilon). \tag{6}$$

The parameter ε prevents the metric to vanish and is set to $\varepsilon = 10^{-3}$ in the numerical tests.

This metric encodes local information about the presence of a vessel at a given position, scale and orientation. The extraction of minimal paths over this metric is a global optimization that links this local information and robustifies vessels extraction.

4

3.2 Distance Map and Geodesic Computation

The length of a lifted curve $\gamma : [0,1] \to \Omega$ over the lifted domain is defined as

$$\mathcal{L}_F(\gamma) \stackrel{\text{def.}}{=} \int_0^1 \rho(\gamma(t))\|\gamma'(t)\| \mathrm{d}t. \tag{7}$$

where the length of the speed vector $v = \gamma'(t) = (v_x, v_r, v_\theta)$ is

$$\|v\|^2 \stackrel{\text{def.}}{=} v_x^2 + \lambda v_r^2 + \mu v_\theta^2, \tag{8}$$

(λ, μ) being normalizing constants that controls the penalty on scale and orientation variations along the vessels in the images. They are set to $\lambda = 0.5$ and $\mu = 0.1$ in numerical experiments. In practice we observed strong robustness with respect to the choice of (λ, μ).

Given a set $\mathcal{A} \subset \Omega$ of seeds points and a set $\mathcal{B} \subset \Omega$ of ending points, a shortest lifted curve $\gamma^*(t) \subset \Omega$ joining $\mathcal{A}$ to $\mathcal{B}$ is defined as a shortest path for the metric $\mathcal{L}_F$

$$\gamma^*(\mathcal{A}, \mathcal{B}) = \underset{\gamma \in \pi(\mathcal{A}, \mathcal{B})}{\operatorname{argmin}} \mathcal{L}_F(\gamma), \tag{9}$$

where $\pi(\mathcal{A}, \mathcal{B})$ is the set of curves γ such that $\gamma(0) \in \mathcal{B}$ and $\gamma(1) \in \mathcal{A}$. The corresponding geodesic distance is $d_F(\mathcal{A}, \mathcal{B}) = \mathcal{L}_F(\gamma^*)$. This definition can be specialized to a single starting point $\mathcal{A} = \{\omega_0\}$ and/or to single ending point $\mathcal{B} = \{\omega_1\}$ to define the geodesic distance between points and/or sets, e.g. $d_F(\omega_0, \omega_1) \stackrel{\text{def.}}{=} d_F(\{\omega_0\}, \{\omega_1\})$.

In practice, γ^* is estimated as follows [44]: the distance to the seeds $\mathcal{A}$ is the geodesic action map $\mathcal{U}_\mathcal{A}(\omega) = d_F(\mathcal{A}, \omega)$ is the unique viscosity solution of the Eikonal equation

$$\forall \omega \in \Omega, \quad \|\nabla \mathcal{U}_\mathcal{A}(\omega)\| = \rho(\omega), \quad \text{with} \quad \forall \omega \in \mathcal{A}, \ \mathcal{U}_\mathcal{A}(\omega) = 0 \tag{10}$$

$$\text{where} \quad \nabla \mathcal{U}_\mathcal{A} = \left(\frac{\partial \mathcal{U}_\mathcal{A}}{\partial x}, \lambda \frac{\partial \mathcal{U}_\mathcal{A}}{\partial \theta}, \mu \frac{\partial \mathcal{U}_\mathcal{A}}{\partial r} \right)^{\mathrm{T}},$$

and where one has to be careful about computing the derivatives with respect to θ modulo π.

Calling $\omega_1 \in \mathcal{B}$ the point in $\mathcal{B}$ with lowest distance to $\mathcal{A}$, the geodesic curve γ^* between $\mathcal{A}$ and $\mathcal{B}$ is then obtained by a gradient descent of $\mathcal{U}_\mathcal{A}$

$$\frac{\mathrm{d}\gamma^*}{\mathrm{d}t}(t) = -\nabla \mathcal{U}_\mathcal{A}(\gamma^*(t)) \quad \text{with} \quad \gamma(0) = \omega_1 \tag{11}$$

Numerical computations. The numerical computation of $\mathcal{U}_\mathcal{A}$ on a discrete grid of $N \stackrel{\text{def.}}{=} n^2 n_r n_\theta$ 4D-points is done in $O(N \log(N))$ operations with the Fast Marching algorithm of Sethian [43]. This algorithm solves an upwind finite difference discretization of (10) with an optimal ordering of the grid points. This ordering corresponds to a front propagation that starts from $\mathcal{A}$ and progressively propagates the values of $\mathcal{U}_\mathcal{A}$ in increasing order. The orientation dimension $\theta \in [0, \pi)$ is handled with periodic boundary conditions $0 \simeq \pi$. A first order Euler-scheme was used to perform the gradient descent. Note that γ^* is computed with sub-pixel accuracy.

3.3 Shortest Paths and 4D curves

A 4D curve $c(x, x')$ between two points $x, x' \in [0,1]^2$ is computed as a 4D geodesic in Ω between the 4D lifted sets $\mathcal{A}(x)$ and $\mathcal{A}(x')$ defined as

$$\mathcal{A}(x^{(')}) \stackrel{\text{def.}}{=} \left\{ (x^{(')}, r, \theta) \setminus r \in [r_{\min}, r_{\max}], \theta \in [0; \pi) \right\}. \tag{12}$$

The 4D curve is then defined

$$c_{x,x'} \stackrel{\text{def.}}{=} \underset{\gamma \in \pi(\omega, \omega'), \omega^{(')} \in \mathcal{A}(x^{(')})}{\operatorname{argmin}} \mathcal{L}(\gamma). \tag{13}$$

This 4D curve contains three components $c_{x,x'}(t) = (\tilde{x}(t), r(t), \theta(t))$. The path $\tilde{x}(t) \subset [0,1]^2$ is the actual centerline over the image plane, whereas $r(t)$ and $\theta(t)$ give the local width and orientation of the vessel, see Figure 4. These orientation and scale are important in medical applications, for instance to compute the local blood flow or to detect tissue diseases.
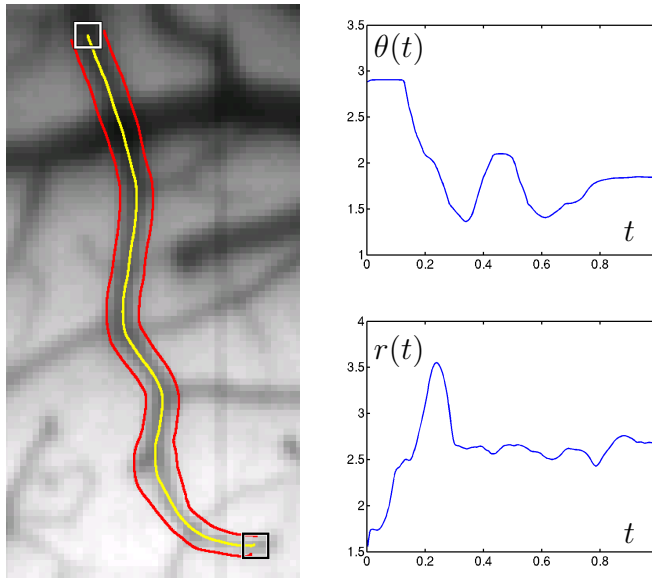
5

Figure 4: *Left:* centerline extraction of a vessel in a cortical image. Starting point: white square. Ending point: black square. *Right:* corresponding orientation $\theta(t)$ and radius $r(t)$.

4 Evaluation of the Geodesic Centerlines

The accuracy of the centerline extraction is compared to two other methods on both synthetic and real data.

- In [8], a 2D metric is computed from an image intensity blurred with a Gaussian filter. The filtering helps to re-center the geodesic since the smoothed image exhibits a local maxima around the center of the vessels, at the cost of a loss of spatial resolution. The smoothing intensity is optimized to give the best results in each test.

- In [28], a 3D (space+scale) metric is computed. All the parameter of this 3D model are optimized to give the best results.

In the experiments, our method was used with an absorbtion parameter $\alpha = 0.1$, which is not optimezed to fit the α of real or benchmark images.

4.1 Evaluation on Synthetic Crossings

The 4D lifting (4) is challenged by testing the extraction of a curved vessel with a self crossing. Figure 5 shows that the vessel curve is not correctly extracted with a metric that does not take into account the local orientation. A 2D purely spatial metric extracts a curve that is not well centered and does not capture the correct topology of the vessel. A 3D space+scale metric correctly centers the geodesic in the vessel but fails to detect the crossing singularity. Our 4D centerline position+scale+orientation favors the extraction of a longer curve that is both well centered and geometrically faithful to the true vessel.

4.2 Accuracy and robustness to noise

The precisions of the three algorithms are tested on several phantoms images, for which the centerlines positions and radii have known analytical forms with sub-pixelic accuracy. The cross section of these phantoms corresponds to the model (1) with parameter $\alpha = 0.01$. An additive Gaussian white noise with various amplitudes are added to the phantoms. Ten phantoms are generated for each condition, and each noise level, see Figure 6. In each case, the true starting and ending points of each phantom are used, as well as the true starting and ending radii for the [28] method.

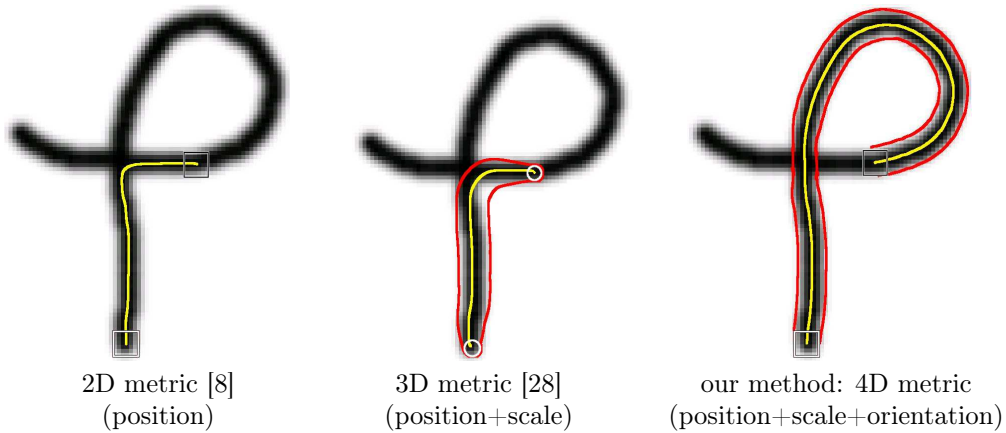|		
2D metric [8]	3D metric [28]	our method: 4D metric
(position)	(position+scale)	(position+scale+orientation)

Figure 5: Comparison of the 2D [8], 3D [28] and 4D lifting (our method) when encountering a self-crossing.
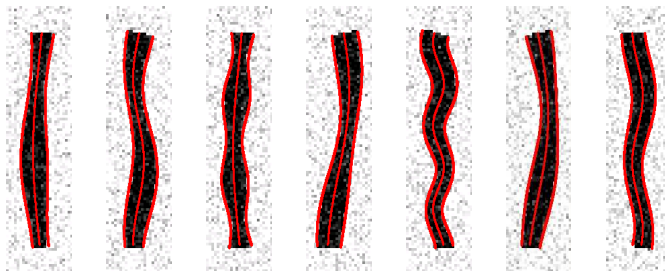

Figure 6: Some of the sample phantoms used in our benchmark (basic intensities range from 0 to 1), shown here with a spatially independent Gaussian noise of variance 0.15.

The extracted 4D curve $c(t) = (\tilde{x}(t), r(t), \theta(t))$ is compared to the ground trust c^* using the following errors:

$$\begin{cases} \text{Error}_C(c)^2 = \int_0^1 \|\tilde{x}(t) - \tilde{x}^*(t^*)\|^2 \mathrm{d}t \\ \text{Error}_R(c)^2 = \int_0^1 |r(t) - r^*(t^*)|^2 \mathrm{d}t \end{cases} \tag{14}$$

where t^* is such that $\tilde{x}^*(t)$ is the ground truth centerline point closest to $\tilde{x}(t)$.

Figure 7 shows $\text{Error}_C(c)$ and $\text{Error}_R(c)$ curves for several synthetic images as a function of the noise level. Using the 3D space+scale lifting [28] produces results of varying quality, and requires a careful tuning for each noise level of the parameter to achieve the optimal error rate. [8]with an optimal smoothing provides a precise evaluation of the centerline locations, but without any evaluation of the local radius. Our method provides both positions and radii with more robustness and accuracy.

Robustness to vessel model The dependency of our 4D lifting method with respect to the precise definition of the model $M(x)$ is challenged by testing several values of the α parameter (1).

Table 1 reports the estimation errors Error_C and Error_R for phantoms f generated with $\alpha = 0.01$ and a noise variance $\sigma = 0.2$. The centerlines extracted with models $M(x)$ are computed for a parameter α set to three different values. This shows that the proposed method is able to recover with good accuracy the centerlines positions and radii, even if the vessel model is unknown.

4.3 Evaluation on Medical Images

Figure 8, left, shows vessels extraction for a complex optical imaging of the cortex with several branches and intersections. As expected, the centerlines computed from different ending points are overlapping.